V European Conference on Computational Fluid Dynamics
ECCOMAS CFD 2010
J. C. F. Pereira and A. Sequeira (Eds)
Lisbon, Portugal, 14–17 June 2010

MATHEMATICAL MODELLING OF SUPESONIC FLOW OVER OPEN CAVITY WITH MASS SUPPLY

Natalya N. Fedorova*, Irina A. Fedorchenko†, Marat A. Goldfeld†, Yulia V. Zakharova†

*Novosibirsk State University of Architecture and Civil Engineering
Leningradskaya str., 113, Novosibirsk, Russia, 630008
e-mail: nfed@itam.nsc.ru

†Khristianovich Institute of Theoretical and Applied Mechanics SD RAS
Instituskaya str., 4/1, Novosibirsk, Russia, 630090
e-mail: gold@itam.nsc.ru, irina@itam.nsc.ru, julsemen@itam.nsc.ru

Key words: supersonic flows, turbulence, shocks, mixing

Abstract. *Turbulent supersonic flows in a plane channel with a cavity presenting a model combustion chamber are studied. The work focuses on the fundamental investigations of channel flowfield over an open cavity with ramp aft wall. The flows are investigated experimentally and numerically with / without taking into account the mass supply into the supersonic turbulent boundary layer before the cavity. As an instrument for the numerical study, RANS model complemented with two-equation turbulence model has been chosen. An in-house 2D code developed in ITAM SD RAS (Novosibirsk) along with ANSYS 12.0 facilities were applied. The parametric studies with changing the cavity length to depth ratio and the wall temperature were conducted numerically. The results obtained with two popular two-equation turbulence models are compared. Validation of the computational results is provided by comparison with experimental data.*

1 INTRODUCTION

It is known [1], that an open cavity is considered to be a promising candidate for a scramjet flame-holder. The cavity "traps" vortexes containing hot low-speed gas and, under certain conditions, may serve as an origin of ignition. "Trapped Vortex" ignition concept are based on the estimation of particle residence time that depends to a great extent on the cavity geometry, number and sizes of the vortexes and the mass exchange with the main flow.

The paper presents the results of the on-going joint experimental and computational studies of high-enthalpy supersonic flows in a channel with abrupt expansion. It focuses on the fundamental investigations of channel flowfield over an open cavity with ramp aft wall. It is known from the previous research [2], that such a cavity is the good candidates for flame-holding in supersonic flow since it provides stable combustion with low pressure drag. The cavity depth h and length L have to be chosen to provide the required residence time and volume of radicals to initiate and sustain the ignition.

2 GEOMETRY, FLOW PARAMETERS, EXPERIMENTAL AND COMPUTATIONAL METHODS

The experiments were conducted at ITAM SD RAS in the IT-302M hotshot wind tunnel with arc heating. The experimental channel has a rectangular cross-section. The model consists of the injector and expanding sections (Fig. 1, a). Injector section (Fig. 1, b) represents a module, which will be weighted by means of the balance. Cavity was installed on the top wall of the first section. The experimental model has the special insertion for gaseous fuel injection into the channel before the cavity forward wall. The cavity aft wall and injection insertion can clearly be seen in Fig. 1, b through an open visualization window.

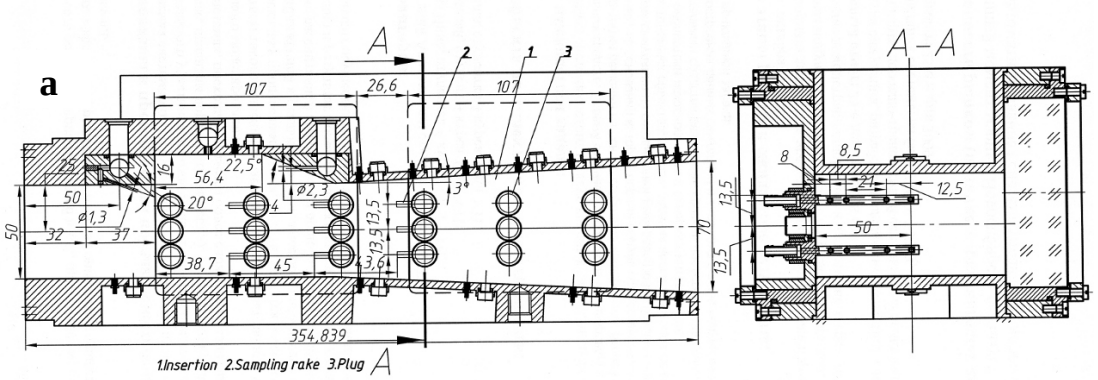

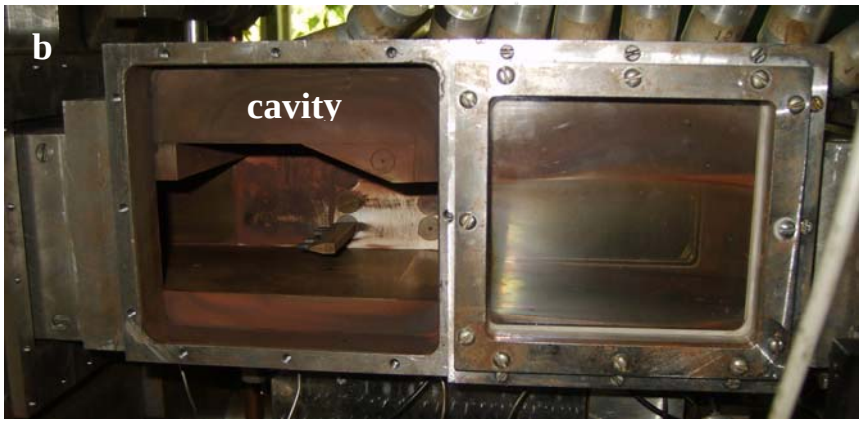

Figure 1: Sketch of the experimental model (a) and photo of the injector section.

The design of the model permits to measure the concentration by means of direct sampling of gas in the channel. To provide optic measurements, the model has windows that allow carrying out the Schlieren visualization of the flow structure. Static pressure and heat fluxes distributions along the channel were measured on the top and bottom walls of the model. Totally, 35 static pressure strain gages and 31 heat flux gages were used.

The typical experimental conditions for the IT-302 facility and incoming gas dynamical parameters are shown in Table 1. Here *P0* is stagnation pressure, *T0* is stagnation temperature; M_e is incoming Mach number, P_e is static pressure, T_e is static temperature, ρ_e is density and U_e is velocity above the boundary layer developed on the channel walls. It should be mentioned that in the real experimental runs, all the parameters are slightly different from those presented in Table 1. Moreover, main flow parameters (*P0, T0* and *Re*) are changing during the experimental run in the short-duration facility.

#	M_e	*P0,* bar	*T0*, K	$Re_1 \cdot 10^6$/m	P_e, bar	ρ_e, kg/m^3	T_e, K	U_e, m/s
1	2	20	1500	33	2.556	1.069	833.3	1157
2	2	30	1500	50	3.834	1.66	833	1157
3	2.5	30	1800	30	1.755	0.765	800	1417
4	3	30	2000	19	0.817	0.398	714	1600
5	3	40	2300	21	1.1	0.62	821	1723

Table 1: Gas dynamical parameters of flows under investigation.

The computations have been performed under the conditions presented in Table 1 for simplified 2D channel geometry shown in Figure 2. Here *h* is cavity depth, *L* stands for cavity length, θ is aft angle and *d* is channel width. For the computational convenience, the cavity was placed on the bottom of the channel. The geometrical parameters of configurations considered in the computations are shown in Table 2. The simplified channel has no the expansion section downstream the cavity and the cavity length was different from that in the real model.

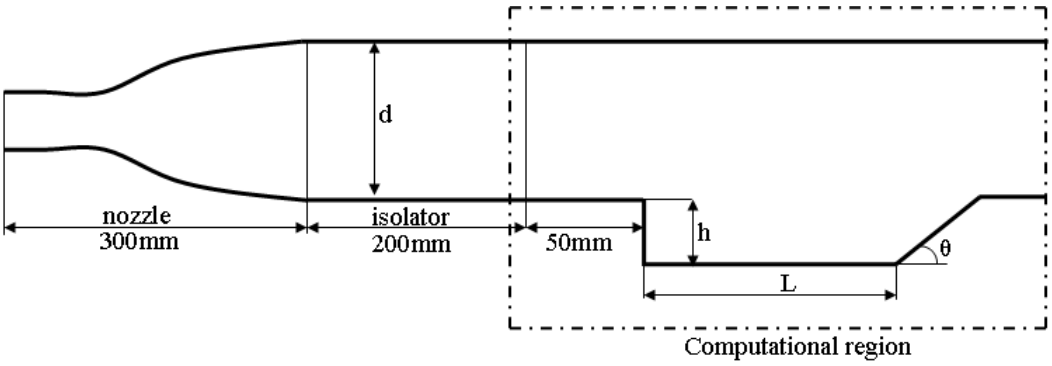

Figure 2: Simplified experimental model used for present computations.

#	*h*, mm	*L/h*	θ,°	*d,* mm
1	16	4.5	22.5	50
2	16	4.5	45	50
3	16	8	45	50

Table 2: Geometrical parameters of a cavity

The computational domain does not include the whole channel but the part of it adjusted to the cavity (Fig. 2). In the most of the computations, the entrance section of the computational domain was chosen at distance of 100 mm upstream of the cavity front wall. The computations in the channel with a cavity were conducted with the help of in-house computer code for solving non-stationary averaged Navier-Stokes equations complemented with the two-equation k-ω [3] and SST [4] turbulence models. For a temporal approximation, a four-step finite-difference scheme of splitting according spatial variables was used [5]. At each fractional step the finite-difference scheme was realized by scalar sweeps. The TVD-scheme of Flux Vector Splitting by van Leer of the third order of accuracy has been used for the approximation of convective terms. The viscous terms have been approximated with the central finite-difference relations of second order of accuracy. Previously, the computer code was successfully applied for modeling the Shock Wave /Boundary Layer Interactions in such configurations as impinging shock wave [6], inlets [7], backward-facing step [8] *etc*.

Two-component flow calculations presented in the paper have been obtained with ANSYS CFD 12.0 instrumentation. The simulation of 2D flow has been carried out on density-based Navier-Stokes coupled solution. The standard k-ω turbulence model applied in ANSYS FLUENT has been used. Both implicit and explicit time methods have been applied during the computations.

At the entrance of the computation domain, the profiles of gas-dynamic and turbulence parameters were set defined from the numerical solution of the problem of the boundary layer development along the channel walls. As the experimental measurements at M=3 presented in Fig. 3 show, the boundary layer thickness at the entrance of test section was about 10 mm. The same thickness was achieved in the boundary layer computations at $x \approx 0.8$ m. The profiles of all the turbulent and gas-dynamics parameters taken from this section were set at the entrance of computational domain of the cavity computations near the top and bottom channel walls.

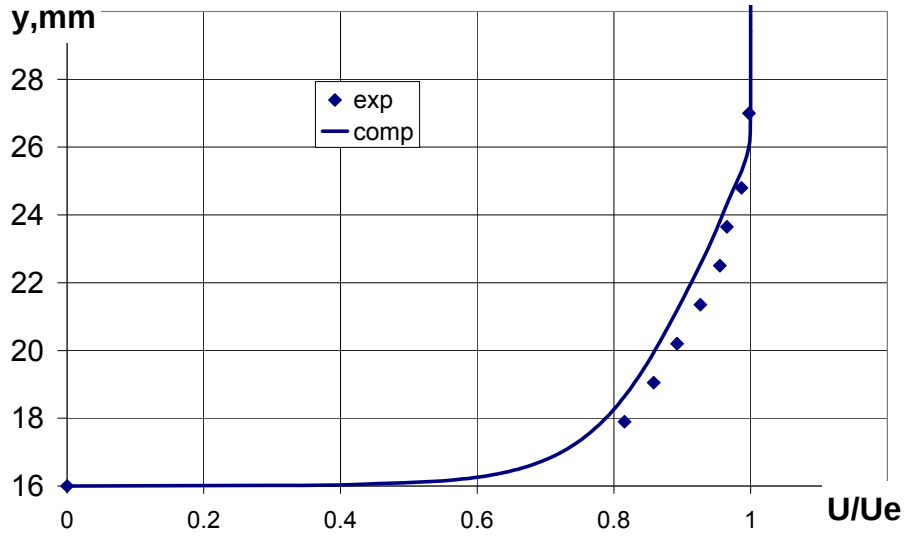

Figure 3: Experimental and computed mean velocity profile in the boundary layer at the entrance of computational domain.

In the computational domain, the regular grid was constructed with quadrilateral cells. The grid was condensed towards to the channel and cavity walls. The typical grid example is shown in Fig. 4. As a rule, grids consist of 650 cells in x direction and 200

cells in y direction. About 50 cells lay in the boundary layer on the top and bottom channel walls.

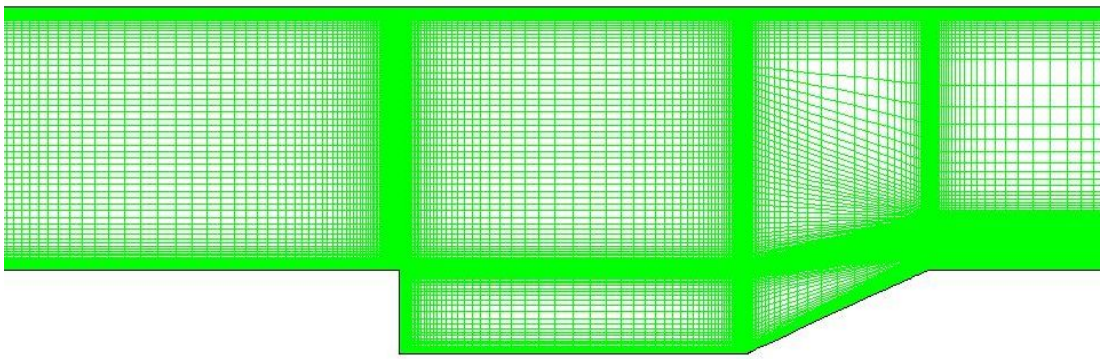

Figure 4: Computational grid for channel with a cavity.

3 NUMER ICAL RESULTS ON CAVITY FLOW WITHOUT MASS SUPPLY

The goal of these computations is a preliminary investigation of the typical flow patterns in the channel with a cavity under conditions presented in Table 1.

3.1 Grid convergence results

To check the grid convergence, a series of the computations was performed with grid refinement in *y* direction. Grid parameters are shown in Table 3. This computations were performed for geometrical configuration #2, flow conditions #2.

Grid	Total cell number	Minimal *y*-step size, m	Maximal *y*-step size, m
Coarse	65000	$2\cdot10^{-6}$	$4.8\cdot10^{-3}$
Intermediate	130000	$1\cdot10^{-6}$	$2.3\cdot10^{-3}$
Fine	4353000	$5\cdot10^{-7}$	$2.3\cdot10^{-3}$

Table 3: Grid parameters

The results of computation on the three grids are shown in Fig. 5. It can be seen that the intermediate grid gives the results that slightly differ from those on the fine grid. So most of results presented were performed on the intermediate grid. It must be noticed that the main difference between results obtained on the coarse and intermediate is due to inadequate boundary layer resolving near the channel walls.

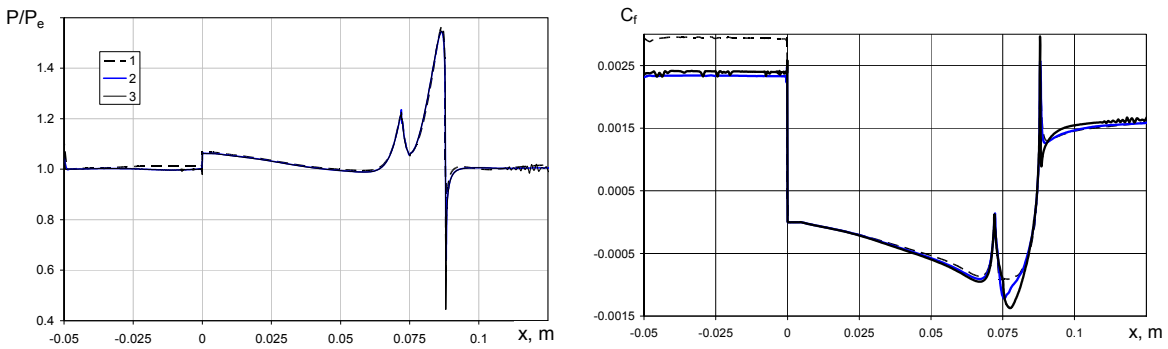

Figure 5: Computational pressure (a) and skin friction coefficient (b) distributions
1 – coarse grid, 2 – intermediate grid, 3 –fine grid

3.2 Computational results at various Mach numbers

The simulation results for cavity geometry #1 were performed at various incoming Mach numbers. In Fig. 6, the computed Mach number fields are shown for cases 1, 3 and 4 of Table 1. In Fig. 7 the computed static pressure distributions along the channel bottom wall are presented. The pictures exhibit flow pattern typical for an open cavity (Fig. 6, b). Before the cavity region, the turbulent boundary layer (1) is developing on the top and bottom walls of the channel. On the cavity forward face, the boundary layer separates forming the mixing layer (2) that falls on the cavity aft wall. In the reattachment region, the compression wave arise that further form the shock (3). Inside the cavity the flow is subsonic. Depending on geometry and flow conditions, the expansion wave or shock may origin from the external corner at the cavity forward wall. For the cases presented in Fig. 6, it is expansion wave that is confirmed by Fig. 7.

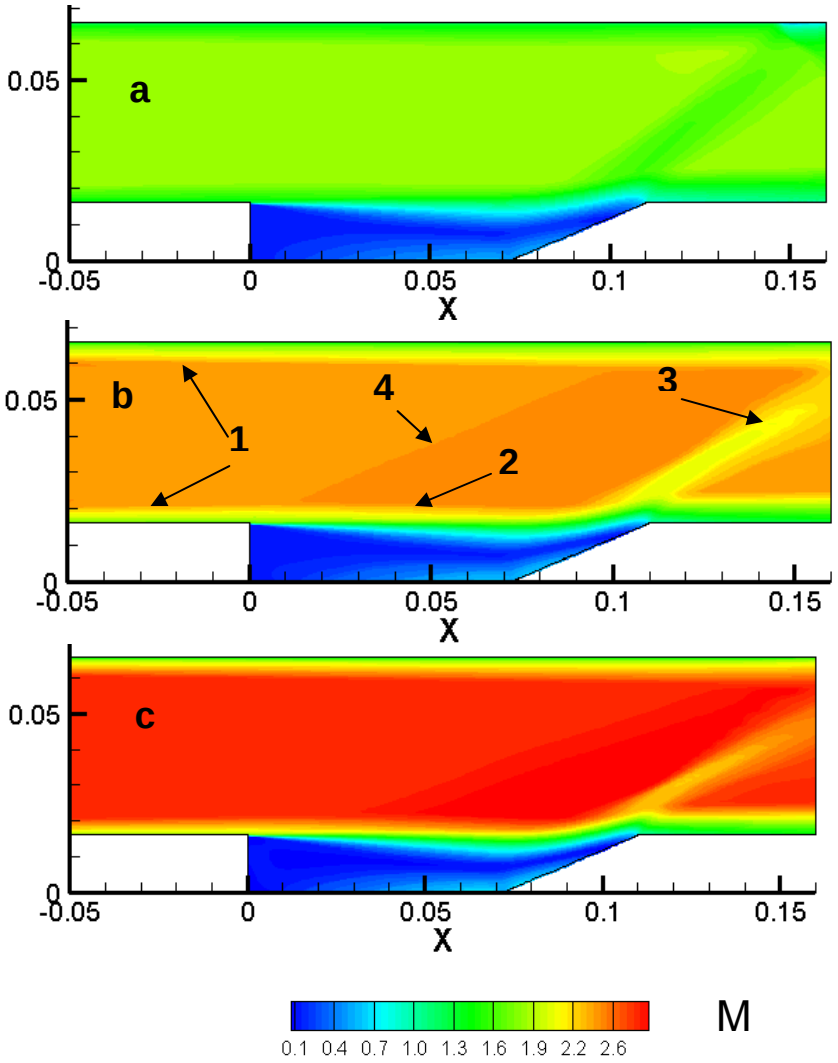

Figure 6: Computed Mach number fields for M_e=2 (a), M_e=2.5 (b) and M_e=3 (c)

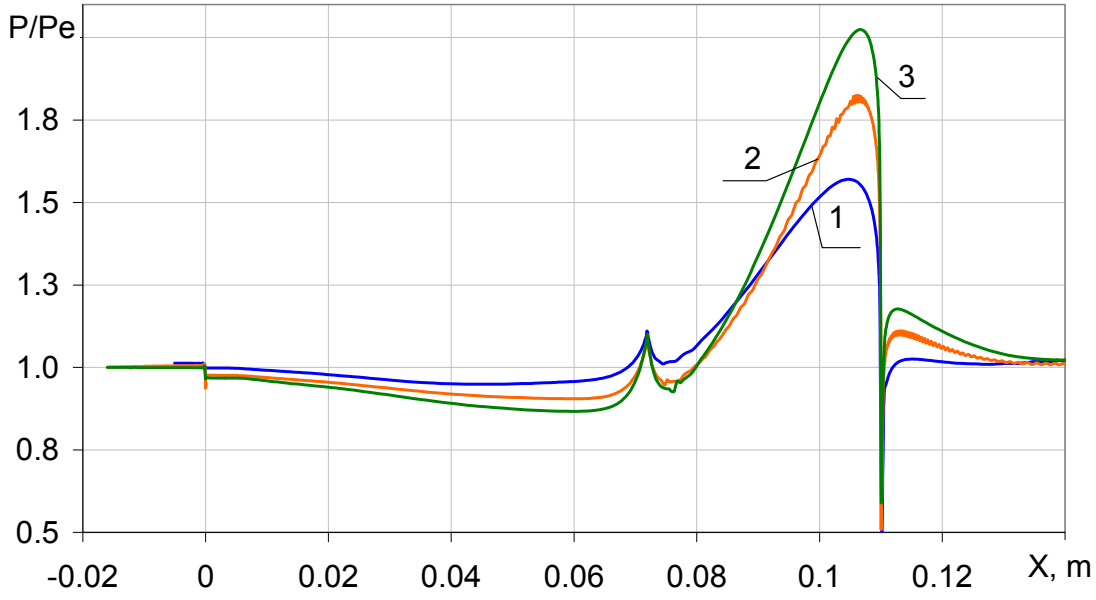

Figure 7: Computed static pressure distributions for M_e=2 (1), M_e=2.5 (2) and M_e=3 (3)

3.3 Simulation results for various cavity length

For flow conditions #1, the computations have been carried out for various cavity lengths (geometry #2 и #3). Results are presented in Figs. 8 - 10. Analysis of static pressure distributions along the cavity wall (Fig. 8) shows that after the cavity front wall the pressure increases in a case of cavity with shorter length, while for a longer cavity it decreases. It is confirmed also by Fig. 9, where the static pressure fields are shown. The effect may be explained by different circumstances of mixing layer development. Figure 10, in which the Mach number fields are presented, shows that for a longer cavity the mixing layer goes down in the centre of cavity that leads to flow expansion. For a shorter cavity, on the contrary, the boundary layer thickness increases in vicinity of cavity front wall and, consequently, static pressure is increasing. The whole wave structure in the channel changes because instead of expansion wave, shock comes to the upper channel wall that, under certain conditions may cause the boundary layer separation and significant pressure rise and even a channel unstart.

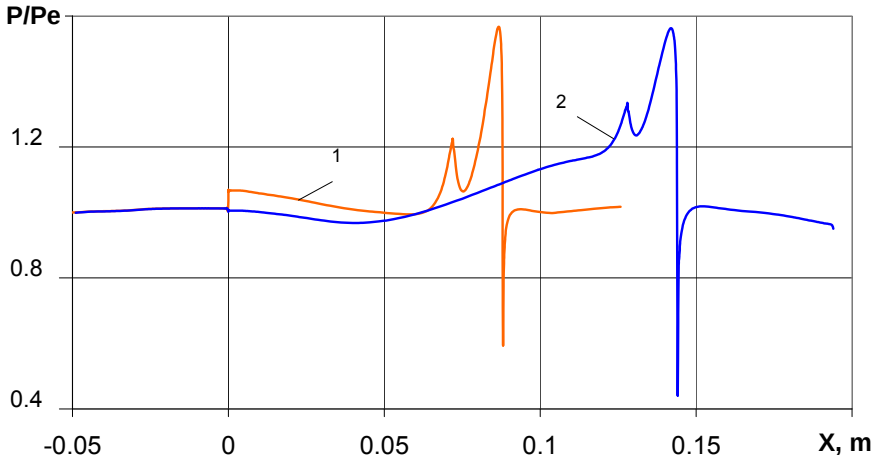

Figure 8: Static pressure distributions for various cavity lengths: *L/h*=4.5 (1) and 8 (2).

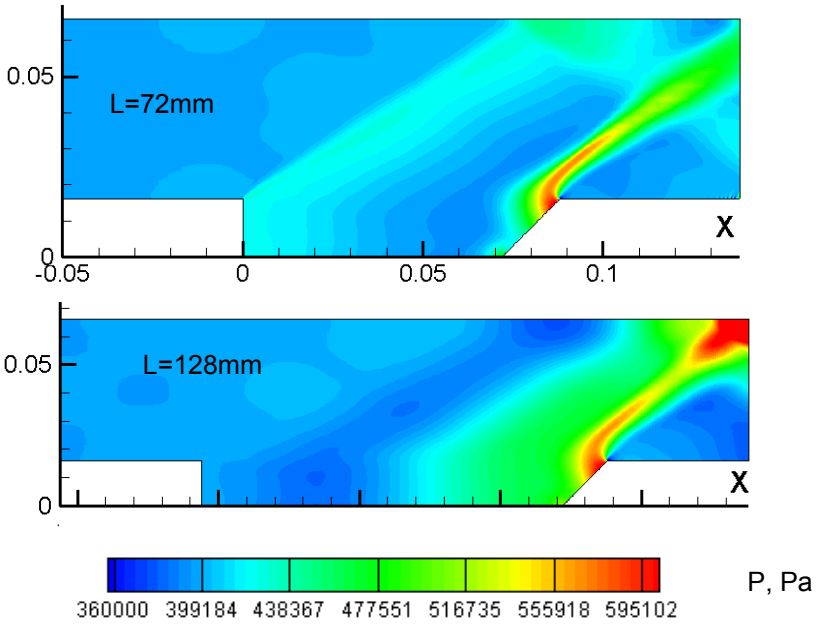

Fig. 9. Static pressure fields for flow condition #1 at cavity length variation

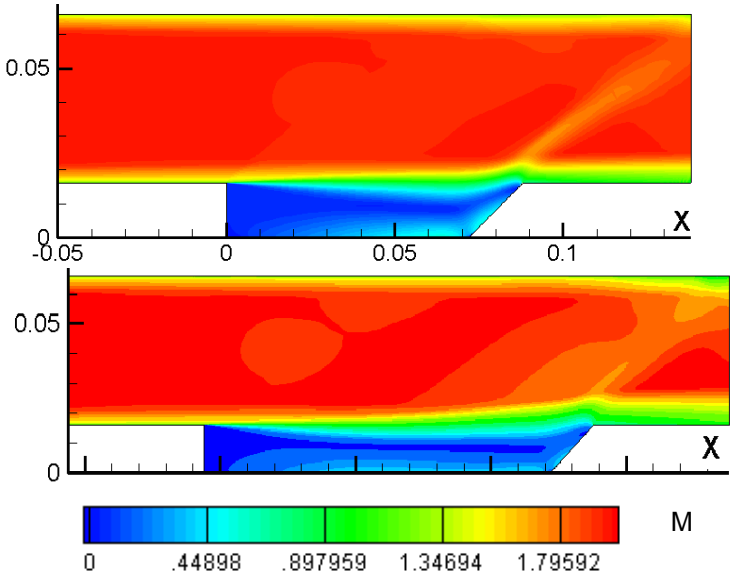

Fig. 10. Mach number fields for flow condition #1 at cavity length variation

3.4 Study of temperature factor influence

For cavity geometry #1, flow condition #4, the study of the wall temperature variation is conducted under adiabatic wall conditions (1) and for T_w=1500K (2), T_w=1000 (3) and T_w= 300 K (4). The results are presented in Figs. 11 and 12. The computations have shown, that under «cold wall» conditions, that are typical for experiments in short duration facility, static temperature in the cavity is significantly lower that that for adiabatic case. For flows with burning, when the cavity servers as a flame-holder, this factor may cause the longer ignition delay time and must be taken into account in planning the experimental conditions.

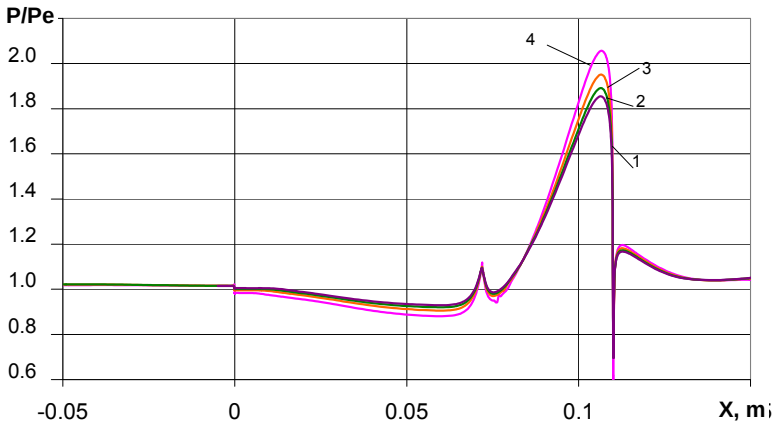

Fig. 11. Computed static pressure distributions at wall temperature variation:

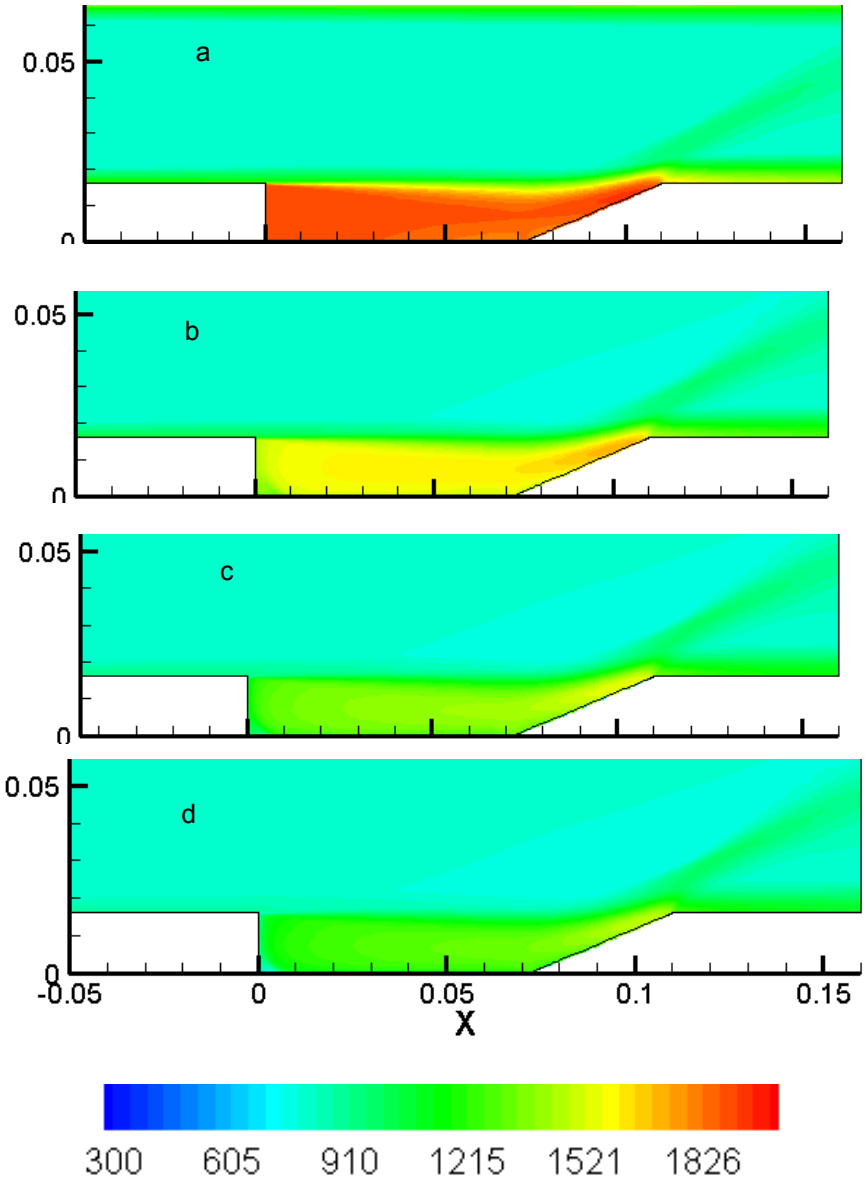

Fig. 12. Computed temperature fields for flow #4 at wall temperature variation: adiabatic wall (a), T_w= 1500K (b), 1000K (c) and 300K (d)

4 SIMULATION OF CAVITY FLOWS WITH MASS SUPPLY

In experiments, the mixing process in a channel with cavity was examined for different injected gases. Primary, non-reacting helium was injected through round holes of 2 mm diameter disposed at 25 mm distance upstream of the cavity front edge. Three holes were equally distributed in span direction of about 100 mm. As a first approximation to the experimental conditions, the 2D slot injection was modeled in the computations for two different injected gases: air and helium.

4.1 Flow with air jet

Numerical simulation of the cavity flow with mass supply has been provided in 2D approach. As the first approach an air injection at x=-25 mm into the channel flow has been realized. The freestream Mach number is equal to 2.8, density 0.676 kg/m^3, jet flow static pressure is 500000 Pa, jet static temperature is 250K, and in order to keep the experimental mass flow rate the Mach number of the jet is taken to be 3.33. Static pressure field obtained in the calculations is presented in Fig. 13, a. The separation shock (*1*) is arisen ahead of the separation bubble organized by the jet issue. It reflects later from the upper wall and forms the reflecting shock (*4*). Behind the jet the flow reattachment takes place and the rarefaction fan (*2*) emerges which interacts with the reflecting wave (*4*) and meets the upper wall of the channel afterwards.

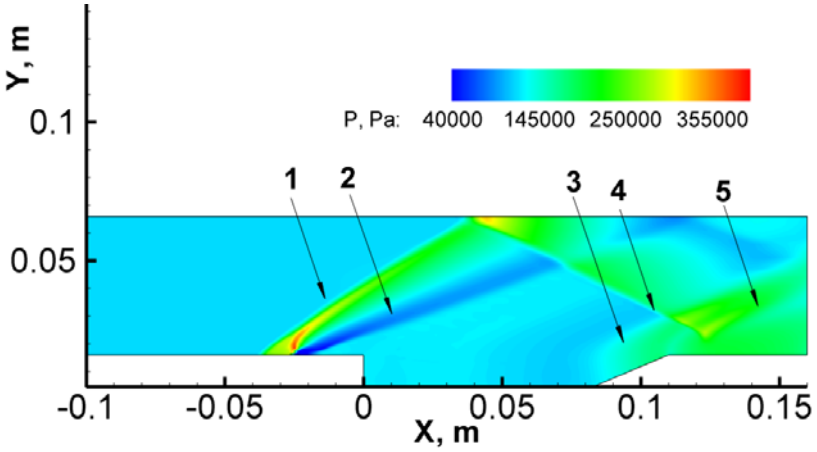

Fig. 13, a Computational pressure field for the cavity case.

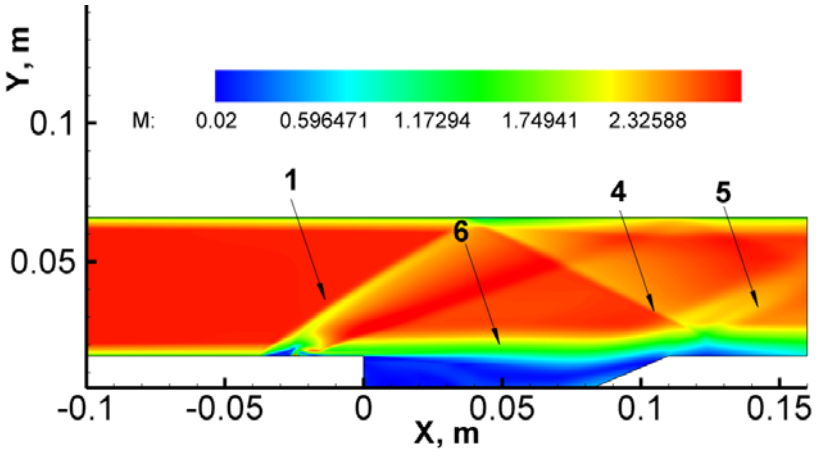

Fig. 13, b Computational Mach field for the cavity case with the air jet.

Subsonic areas of the flow are located in the cavity where the big re-circulating zone is organized and in front of the jet where a strong stagnation of the flow is appeared as can be seen from the Mach number distribution (Fig. 13, b). At the aft wall of the cavity where the mixing layer (*6*) falls onto the wall the compression wave (*3*) is formed (Fig. 13, a). It interacts with the reflected shock (*4*) and goes further downstream along with the reflected shock wave (*5*).

The zoomed picture of the jet issuing into the supersonic flow is drawn in Fig. 14. Here the streamtraces of the configuration are shown together with the vertical velocity field. Two vortexes of opposite direction of rotation are located in front of the jet and one recirculation zone is appeared behind it. Separated and recompression shock waves can be clearly seen here.

The wall pressure distribution is presented in Fig. 15. Pressure peak is corresponding to the jet pressure level and the pressure plateau ahead of it conditioned by the separation shock is visible. Low values of the pressure are observed in the rarefaction zone behind the jet. Further downstream almost constant pressure level is kept through the cavity and after that the pressure rise takes place due to the presence of the compression wave (*3*) and the reflection of the shock (*4*) according to the notation of Fig. 13.

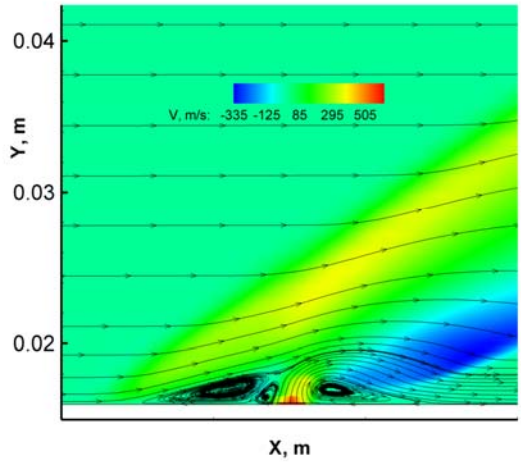

Fig. 14 Streamtraces of the flowfield in vicinity of the jet location

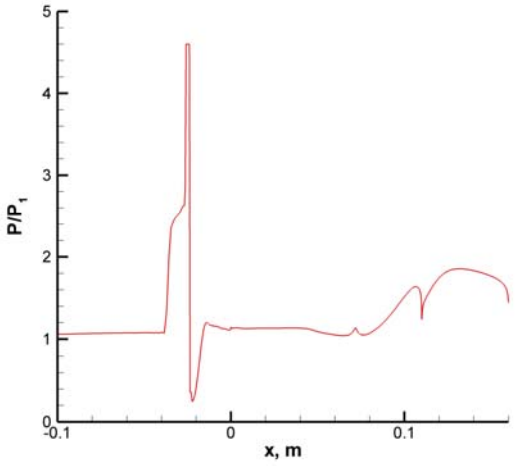

Fig. 15 Wall static pressure distribution related to the freestream pressure

4.2 Flow with helium jet

The helium injection has been modeled at the same freestream parameters. The static pressure of the jet is $5 \cdot 10^5$ Pa, the static temperature is 220K and the jet exit Mach number is about 1. The main flow structure remains similar to the air jet flowfield described above as can be seen in Fig. 16, a where the pressure field is presented. The separation shock can be observed which reflects from the top wall and interacts with the contact boundary of the air-helium mixture. Since the last has a lower density than the outer air flow the rarefaction wave reflection appears in vicinity of the tail part of the cavity.

Distribution of mass fraction of helium shows good mixing level inside the cavity, and the location of the reflected shock wave is indicated by the layer increase.

Nevertheless further downstream of the cavity the volume occupied with the mixture has no tend to increase and is located at the bottom part of the channel.

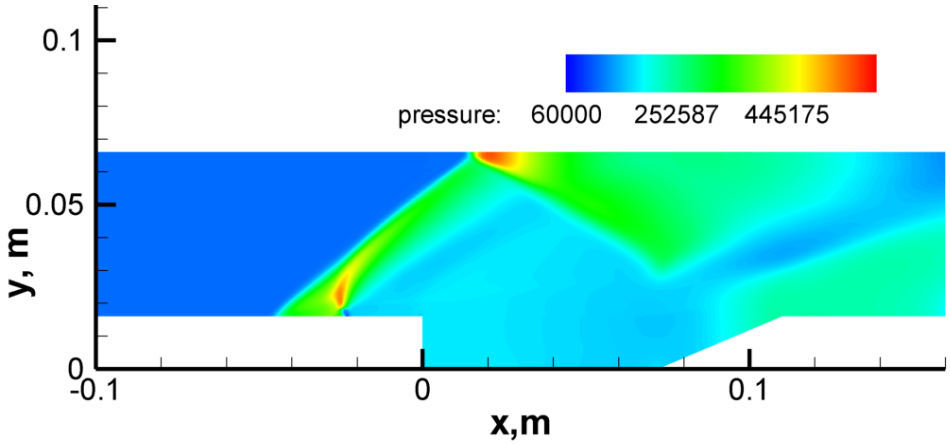

Fig. 16, a Computed pressure field for the cavity case with the helium jet.

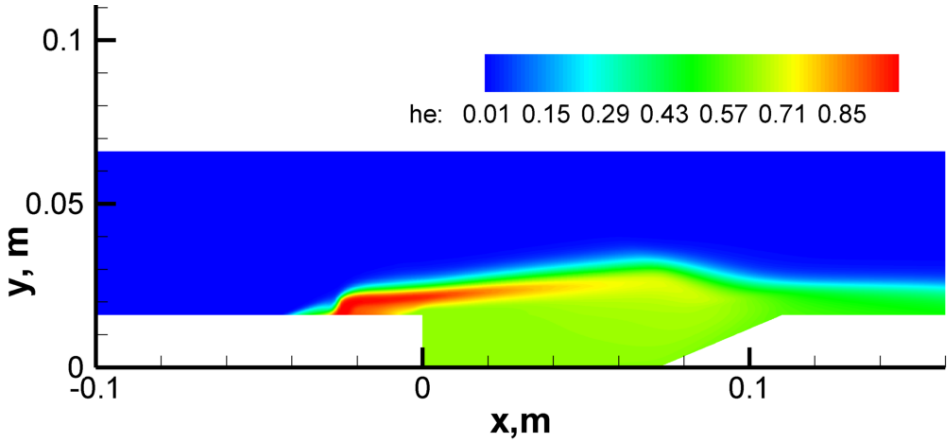

Fig. 16, b Computed helium fraction distribution for the cavity case with the helium jet

5 CONCLUSIONS

- High-speed high-enthalpy flows in a channel with cavity of open type have been investigated experimentally and numerically in a wide range of incoming flow conditions;
- Series of computations have been performed in a frame of Reynolds averaged Navier-Stokes equations using in-house software and ANSYS Fluent instrumentation;
- Cavity flows was modeled taking into account air and helium injection into the supersonic flow;
- Typical flow patterns were studied numerically under conditions of experimental facility for 2D simplified channel geometry. It was shown that different flowfield structure may occur in the channel depending on the situation in vicinity of the cavity front edge;

- Parallel to the computations, experimental model was designed and manufactured and experimental runs were performed for flows with/without gas injection;
- Further computations plan include simulation of the flow for the real geometrical and gas-dynamic parameters.

6 ACKNOLEDGEMENTS

The work has been financially supported by Ministry of Education and Sciences of Russian Federation, AVC Program "Development of Scientific Potentials of Higher School", grant #2.1.1/4674 and by Russian Foundation for Basic Research in a frame of grant #09-08-01001-a.

REFERENCES

[1] A. Ben-Yakar, R.K. Hansin, Cavity Flame-Holders for Ignition and Flame Stabilization in Scramjets, an Overview, *Journal of Propuls. Power* **17**, No. 4, pp. 869-878 (2001)

[2] M. R. Gruber, R. A. Baurle, T. Mathur, K.-Y. Hsu, Fundamental Studies of Cavity-Based Flameholder Concepts for Supersonic Combustors, *Journal of Propulsion and Power*, **17**, pp. 146–153 (2001)

[3] D.C Wilcox, Turbulence modeling for CFD, DCW Ind. Inc., La Canada, California (1993)

[4] F.R Menter, Two-Equation Eddy-Viscosity Turbulence Models for Engineering Application, *AIAA Journal,* **32**, No. 8, pp. 1598-1605 (1994)

[5] Borisov, A.V., Fedorova, N.N.: Numerical simulation of turbulent flows near the forward-facing steps. *Thermophysics and Aeromechanics*, **4**, No. 1, pp. 69-83 (1996)

[6] N.N.Fedorova, I.A. Fedorchenko, E. Shuelein, Experimental and numerical study of oblique shock wave / turbulent boundary layer interaction at M=5, *Comp. Fluid Dyn. Journ.* **10**, No. 3, pp. 376-381 (2001)

[7] I.A. Bedarev, N.N. Fedorova, M.A. Goldfeld, F. Falempin, Mathematical Modeling of Supersonic Turbulent Flows in Inlets with Rotating Cowl, In: C. Groth, D.W. Zingg (eds) Computational Fluid Dynamics 2004, Springer-Verlag, pp. 295-300 (2006)

[8] I. A. Bedarev, M. A. Goldfeld, Yu. V. Zakharova, N. N. Fedorova, Investigation of temperature fields in supersonic flow behind a backward-facing step, *Thermophysics and Aeromechanics*, **16**, No. 3, p. 355 (2009)